euspen's 23rd International Conference & Exhibition, Copenhagen, DK, June 2023
www.euspen.eu

Influence of head orientation on bead geometry and penetration in wire laser additive manufacturing with coaxial technology

Clément Roch [1], Christophe Tournier [1], Sylvain Lavernhe [1], Adel Abbas [1]

[1]*Université Paris-Saclay, ENS Paris-Saclay, LURPA, 91190, Gif-sur-Yvette, France*

clement.roch@ens-paris-saclay.fr

Abstract
Wire laser additive manufacturing (WLAM) distinguishes itself from other wire based processes by its stability and repeatability of deposited geometry, even at high deposition rates, leading to near net shape parts. While the most common configuration of head technology consists of a single laser beam and wire feeding along two different orientations, other technologies align the feed direction with the energy resulting in a coaxial configuration. This can be achieved by the use of several laser beams placed on a cone around the wire to focus on the virtual tool centre point. Although wire feed angle and direction have been linked to variations in bead dimensions and penetration with a single laser, few articles investigated the head orientation effects with coaxial technologies. This study focuses on the effect of the head orientation to the substrate on bead and penetration profiles using a three lasers coaxial head. The head rotation around its own axis results in varying shapes and penetration profiles and leads to production defects in some configurations. Asymmetrical beads with non-centred penetrations are observed experimentally and linked to the beam's positions relative to the bead direction. A symmetrical arrangement with one laser to the front of the wire and two lasers at the back produces a symmetrical bead with minimal penetration, while an asymmetrical configuration with two lasers on one side of the wire and one on the other results in a displacement of the bead geometry toward the higher irradiance area, with a greater bead penetration. Therefore, the rotation of the coaxial head around its own axis relatively to the travel direction needs to be considered to maintain the control of the deposited material and the stability of the process during the manufacturing of the part.

Additive Manufacturing, Laser Wire, Bead geometry, Penetration

1. Introduction

Metal additive manufacturing enables the development of new production strategies, with several processes already being used. The feedstock material is often either powder or wire, the later resulting in simpler installations and being able to produce large volume parts. Among these wire-based processes, Wire Laser Additive Manufacturing (WLAM) distinguishes itself by the use of a laser beam as energy supply. Different technologies have been developed with some feeding the wire from a different axis as the laser and others feeding from the same axis as the energy, resulting in coaxial configurations. To achieve this coaxial feeding a ring beam [1] or multiple beams placed around the wire [2] can be used.

As most of the experimental setups are unique, manufacturing recipes have to be established for each installation. This is often done in an empirical manner by manufacturing single beads to define correct process parameters then producing overlapping beads before building layers for massive parts or single-bead walls. As the manufacturing process is similar to other welding based processes, the study of single and multiple beads is often shared, leading to several models on bead geometry. The elliptical [3], sinusoidal [4] or polynomial models of degree 2 [5] or 4 [6] are the most common ones, and comparative studies found that most of these models offer a decent representation of the beads [7], while the optimal model depends on the ratio between wire feed speed and travel speed [8]. Therefore most studies only describe the bead geometry by using key dimensions such as bead width W, height H, penetration P, contact angle θ_c, cross-sectional area A and dilution ratio D, and focus on how the process parameters influence these parameters. Three process parameters are commonly studied: laser power, wire feed speed and travel speed, and are linked to process stability. The wire feed speed and laser power are linked together, and providing too much power with low wire feed speed will create dripping, where the wire melts and creates drips instead of a continuous bead, while a low power input compared to a high wire feed speed generates stubbing, where the wire is not fully melted and forces on the substrate creating an irregular geometry [9].

Apart from these 3 main parameters, some parameters of head positioning to the substrate were investigated such as feeding direction for lateral feed. These studies on non-coaxial configurations highlighted the importance of the angle between wire and substrate for process stability and found that front feeding results in smoother beads than back feeding [10]. No similar study was found for coaxial configurations, with most papers focusing on the 3 main parameters. The only positioning parameter mentioned for coaxial setups with multiple beams is the working distance which corresponds to the distance between the beams intersection point and the substrate and influences bead geometry. This effect on bead geometry has been linked to the change in power density generated by variations in the working distance when using 3 laser beams [11]. However, other parameters of head positioning influence the power density, especially for three beams technologies. The head rotation around the wire axis is one of those parameters, as it can place either one or two beams at the front of the melt pool, and create symmetrical or asymmetrical configurations. Moreover, it can vary during manufacturing if the variations in travel directions are not taken into account.

Therefore the study proposed in this paper focuses on the effect of the 3-beam coaxial head rotation on bead geometry and penetration. The experimental setup and manufacturing conditions are presented before describing the method applied. The obtained results in external geometry and penetration are then presented and the effect of head rotation is discussed.

2. Experimental setup

The considered WLAM process uses 3 laser beams to obtain a coaxial configuration. The additive manufacturing head is manufactured by Coaxworks and is paired with an Ytterbium fibre laser source with a maximum power of 4kW from IPG, which generates a beam with a top-hat power profile and a spot size of 2 mm. The head is mounted on an ABB robot arm (Fig 1), while the substrates are placed on a positioner. The material used is IN718 for the 1.2 mm diameter wire while the substrate is S235 JR steel and measure 80 mm in length, 40 mm in width and 10 mm in thickness. Airflow protects the head optics from splatters and smoke and a flow of Argon at 2 bars shields the melt pool. Additionally, a Xiris weld camera is used to monitor the process.

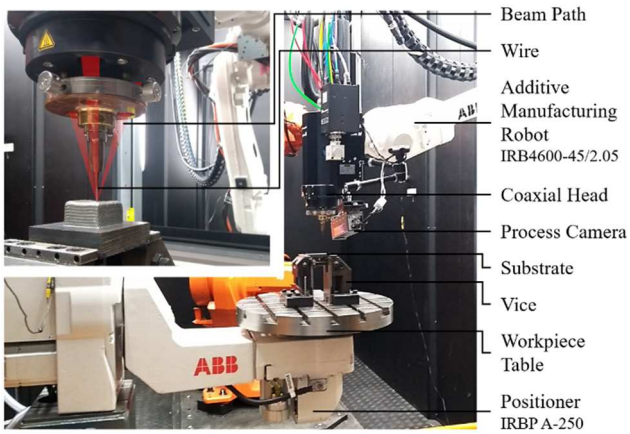

Figure 1. overview of the WLAM setup and close view of the head

The initial laser beam is divided in three beams which are placed at an angle of 17.5° to the head vertical axis (z-axis) and equally spaced around it. Beam 1 is at a 90° angle to the head x-axis, beam 2 at 150° and beam 3 at 30°. The z-axis is placed along gravity and the substrate is placed orthogonaly to it. The working distance is chosen at -2 mm, meaning that the intersection point of the 3 lasers is 2 mm beneath the substrate surface. Figure 2 displays the full laser spot obtained after a laser shot on a painted glass plane. The 3 beams are clearly identifiable on the spot profile.

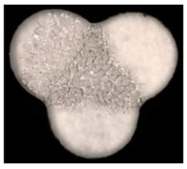

Figure 2. full laser spot on a glass plane at -2 mm working distance

A process window was established for the usual parameters (laser power, wire feed speed and travel speed) in this configuration and displayed dripping or stubbing defects outside of this window. An operating point is defined with a power of 2.2 kW, a wire speed of 2 m/min and a travel speed of 1 m/min.

3. Method

The head rotation along its z-axis relatively to the substrate will be described by the angle α. Technological constraints due to cables management keep it constrained in the interval [-70°;70°]. 5 values were chosen for α: -60°, -30°, 0°, 30° and 60°, which correspond to specific configurations with respect to the travel direction. Figure 3 presents simulations of the laser power density on the substrate for each of these values, with the beam axes numbered and displayed in red, and the profile of the laser spot plotted in black.

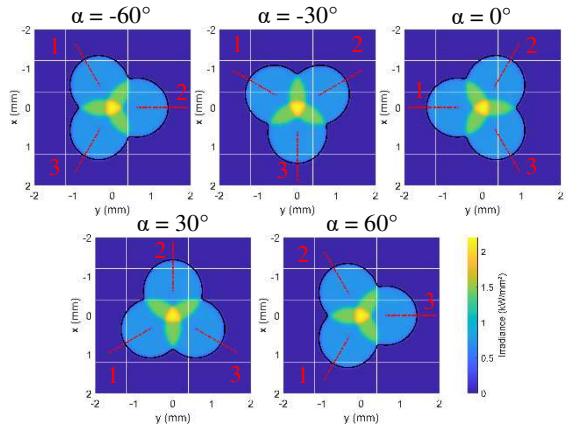

Figure 3. power density and laser spot limit for different values of head rotation

By choosing the x-axis as travel direction, the -30° and 30° both result in symmetrical configurations, while -60°,0° and 60° lead to asymmetrical configurations. Moreover, configurations with α = -60° and 60° both result in similar configurations but with different beams, as beam 2 is aligned with y for -60° while it is beam 3 aligned with y for 60°.

All beads were produced with the parameters of the established operating point. The beads are 45 mm long, spaced 20 mm apart and a waiting time of around 1 minute was kept between each manufacturing, as to reduce possible thermal accumulation effects. Geometries produced under these conditions were found to be independent of manufacturing sequence by preliminary tests.

A Keyence laser line scanner was used to measure the beads external geometry. After identifying the x direction on the measured data, the y-axis was divided into regular intervals between -2 and 2 mm. A local height distribution was then obtained for each value of y corresponding to the variations in height across the entire bead length for this value. For each of these distributions the mean value and standard deviation σ were computed to obtain a statistical mean bead profile. A 95% confidence interval can be considered as ±1.96 σ under the assumption that the values follow a Gaussian distribution.

The bead height H, width W and area A were determined with their confidence intervals by using these statistical profiles. A new value A_r is added to represent the asymmetry found on several bead profiles. It corresponds to the ratio between the area placed right of the bead centre and the total area. The bead centre is considered as the middle of the bead width and is displayed on figure 4 along with the other dimensions on a bead cross section. This value was only determined on the mean profile, therefore no confidence interval is considered.

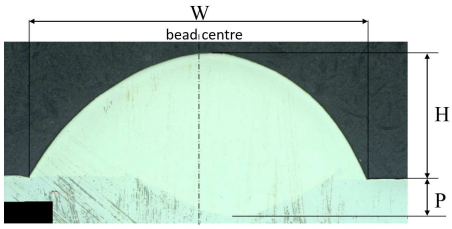

Figure 4. cross section of a bead with its dimensions

After measuring the external geometries, the beads are cut in their middle perpendicularly to the travel direction. The obtained cross-sections are then polished and observed using a metallurgical microscope equipped with a camera. Several images are stitched together to obtain a full view of each bead.

4. Results and discussion

While the established operating point results in smooth beads for most values of α, all beads produced with α = 30° generate stubbing, where the wire is pushing against the substrate. This could be due to beam placement, as having two beams at the front of the melt pool and only one at the back can lead to less power on the melt pool, and thus less power to melt the wire.

The dimensions of the manufactured beads with their associated confidence intervals of ±1.96 σ are displayed on figure 5 as functions of angle α. The effect of stubbing with α = 30° is visible on the confidence interval of each dimension, as it is much wider than any other, which is due to the unevenness of the obtained geometry.

As all beads were produced with the same ratio of wire feed speed to travel speed, bead area (A) is expected to be constant for all values of α. This is observed on figure 5, as all differences in mean values of bead area are inferior to the confidence intervals.

Bead height (H) presents some variations in values which remain relatively small. A tendency to obtain lower heights for symmetrical configurations (α = -30°) and higher values for asymmetrical ones are observed, with heights for -60° and 60° being almost identical.

Bead width (W) also presents some variations, with symmetrical configurations (α = -30°) resulting in the largest bead. All other beads are narrower excepted for α = 30° where stubbing has an important effect on bead width.

Both α = -30° and α = 30° create symmetrical power configurations, as seen in figure 3, with the difference of beam placement to the front or back of the melt pool. Comparing the obtained profiles for these cases on figure 6 shows that they result in similar mean profiles but that the confidence interval represented by dashed lines is wider for α = 30° due to stubbing.

As with bead height, the width for α = -60° and 60° are similar, and comparing both profiles on figure 6 highlights this similarity. This is compatible with the fact that these two values of head rotation generate the same asymmetrical configuration with one beam along the y-axis and the other two on the negative side of y, only changing which beam is on the right.

However, these asymmetrical configurations do not result in the same beads as the symmetrical one (α = -30°), the bead being larger but presenting a lesser height. Moreover, it can be observed that the bead obtained for α = -30° is more

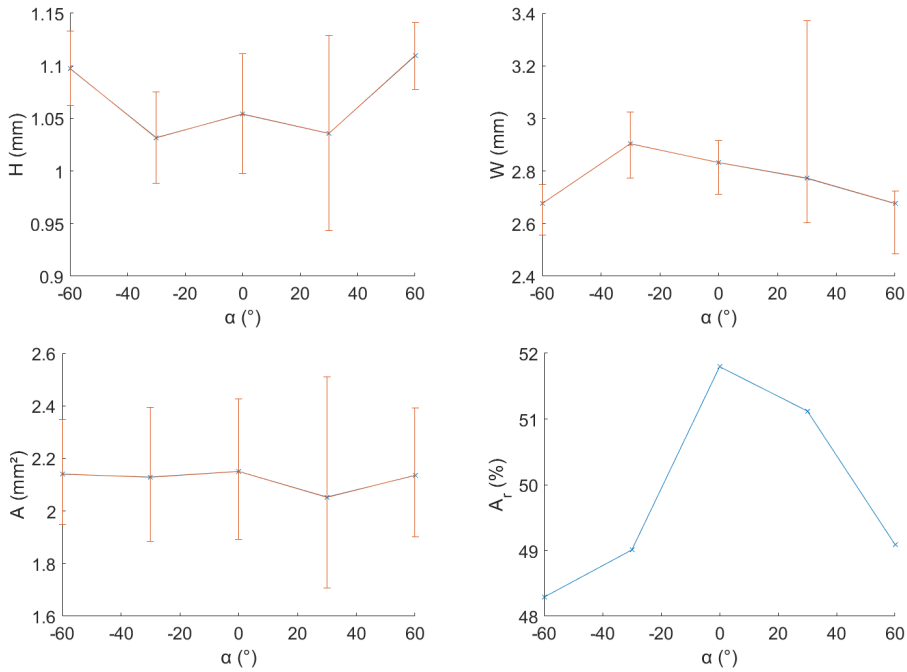

Figure 5. Variations in bead dimensions for different values of head rotation, with evolution along the bead length as confidence intervals

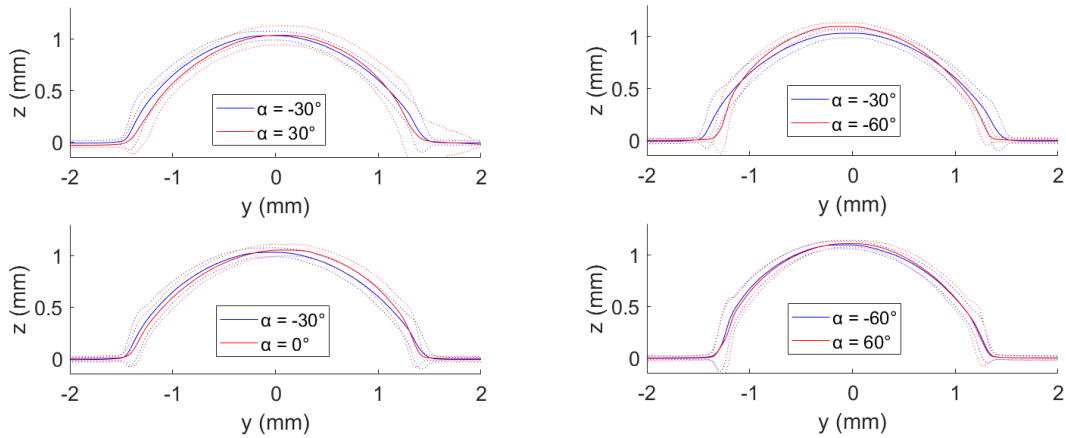

Figure 6. Comparison between bead profiles

symmetrical than the one for α = -60°, which has more matter on the left side. This is seen in the A_r value which indicates that the area on the right is 48.3% of the total area for α = -60°. The right side has more matter when A_r is superior to 50%, which happens for α = 0° when A_r = 51.8%. Comparing both configurations on figure 3 shows that the single laser beam is aligned with -y for α = 0°, which represents an opposite configuration to α = -60°, where it is aligned with +y. It therefore seems that beads produced in asymmetrical configurations present more matter on the side receiving more power.

Comparing α = -30° and α = 0° on figure 6 shows less effect on width and a small increase in height, but isn't as significative a difference as for α = -30° and α = -60°. This could indicate that other parameters than power density also have an effect on bead shape.

Figure 7 presents the beads cross-sections for all values of α with the mean profile and confidence interval being superposed on top. As expected, all the cross-sections fit inside the confidence interval, with the exception of α = 60° for which the height of the cross-section is slightly higher. The observed bead profiles vary from what is typically seen in welding or Wire Arc Additive Manufacturing as they present a low dilution. Moreover, the observed penetration varies between beads with α = -30° having a shallow dilution compared to the asymmetrical configurations. Moreover, the penetration is offset from the bead centre for -60°, 0° and 60°, and always to the side receiving more power.

5. Conclusion

This article studied the effect of head rotation around its vertical axis for WLAM with a coaxial head with 3 beams. Beads were produced for 5 values of head rotation corresponding to different configurations of beam positioning compared to travel directions. Comparison of geometric profiles showed that beads produced in a symmetrical power configuration are more symmetrical than beads produced in asymmetrical configurations, for which more matter is deposited on the side receiving more power. Moreover, an effect of the head rotation on penetration was also observed, with asymmetrical configurations presenting deeper penetration offset to the side receiving more power. Further work could focus on linking the variations in power density to variations in bead geometry as well as investigating the effect of head rotation for bead overlapping and layer building.

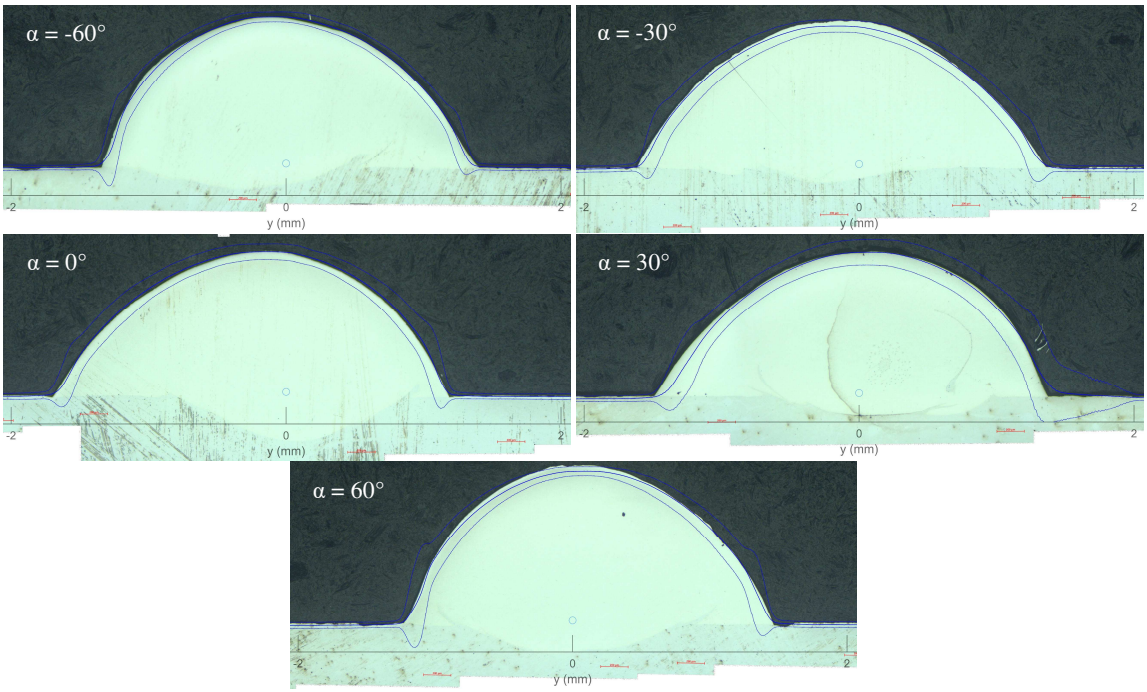

Figure 7. Variations in bead dimensions for different values of head rotation

References

[1] Ayed A, Bras G, Bernard H, Michaud P, Balcaen Y and Alexis J 2020 Study of Arc-wire and Laser-wire processes for the realization of Ti-6Al-4V alloy parts *MATEC Web of Conferences* **321**

[2] Du F et al 2019 Dimensional characteristics of Ti-6Al-4V thin-walled parts prepared by wire-based multi-laser additive manufacturing in vacuum *Rapid Prototyping Journal* **25-5** 849-856

[3] Aiyiti W, Zhao W, Lu B and Tang Y 2006 Investigation of the overlapping parameters of MPAW-based rapid prototyping *Rapid Prototyping Journal* **12** 165-172

[4] Cao Y, Zhu S, Liang X and Wang W 2011 Overlapping model of beads and curve fitting of bead section for rapid manufacturing by robotic MAG welding process *Robotics and Computer-Integrated Manufacturing* **27** 641-645

[5] Suryakumar S, Karunakaran K P, Bernard A, Chandrasekha Ur, Nadella R and Sharma D 2011 Weld bead modeling and process optimization in Hybrid Layered Manufacturing *Computer-Aided Design* **43** 331-344

[6] Kumar M, Kumar S S and Sharma A 2021 Bi-polynomial fourth-order weld bead model for improved material utilization and accuracy in wire-arc additive manufacturing: A case of transverse twin-wire welding *Advances in Industrial and Manufacturing Engineering* **2** 100049

[7] Ding D, Pan Z, Cuiuri D and Li H 2015 A multi-bead overlapping model for robotic wire and arc additive manufacturing (WAAM) *Robotics and Computer-Integrated Manufacturing* **31** 101-110

[8] Xiong J, Zhang G, Gao H and Wu L 2013 Modeling of bead section profile and overlapping beads with experimental validation for robotic GMAW-based rapid manufacturing *Robotics and Computer-Integrated Manufacturing* **29** 417-423

[9] Abioye T E, J. Folkes J and Clare A T 2013 A parametric study of Inconel 625 wire laser deposition *Journal of Materials Processing Technology* **213-12** 2145-2151

[10] Mok S H, Bi G, Folkes J and Pashby I 2008 Deposition of Ti-6Al-4V using a high power diode laser and wire, Part I: Investigation on the process characteristics *Surface and Coatings Technology* **202-16** 3933-3939

[11] Ji S, Liu F, Shi T, Fu G and Shi S 2021 Effects of defocus distance on three-beam laser internal coaxial wire cladding *Chinese Journal of Mechanical Engineering* **34** 45